Comput. Mech. (2006) 38: 390–402
DOI 10.1007/s00466-006-0053-x

ORIGINAL PAPER

**Johan Hoffman**

# Simulation of turbulent flow past bluff bodies on coarse meshes using General Galerkin methods: drag crisis and turbulent Euler solutions

Received: 11 October 2005 / Accepted: 29 January 2006 / Published online: 11 March 2006


**Abstract** In recent years adaptive stabilized finite element methods, here referred to as *General Galerkin (G2) methods*, have been developed as a general methodology for the computation of mean value output in turbulent flow. In earlier work, in the setting of bluff body flow, the use of no slip boundary conditions has been shown to accurately capture the separation from a laminar boundary layer, in a number of benchmark problems. In this paper we extend the G2 method to problems with turbulent boundary layers, by including a simple wall-model in the form of a friction boundary condition, to account for the skin friction of the unresolved turbulent boundary layer. In particular, we use G2 to simulate drag crisis for a circular cylinder, by adjusting the friction parameter to match experimental results. By letting the Reynolds number go to infinity and the skin friction go to zero, we get a G2 method for the Euler equations with slip boundary conditions, which we here refer to as an *EG2 method*. The only parameter in the EG2 method is the discretization parameter, and we present computational results indicating that EG2 may be used to model very high Reynolds numbers flow, such as geophysical flow.

**Keywords** Navier-Stokes equations · Euler equations · Approximate weak solution · Weak uniqueness · General Galerkin G2 · Skin friction boundary condition · Finite element method · A posteriori error estimate · Duality

## 1 Introduction

The Navier–Stokes equations seem to give an accurate description of a great variety of fluid flows, including both *laminar flow* with ordered flow features and *turbulent flow* with smaller and larger vortices in a complex interaction. Even though the Navier–Stokes equations have been known for almost 200 years, the basic mathematical questions of existence and uniqueness stand without answers, and computational simulation of turbulent flow is to a large extent still considered an outstanding open problem.

In earlier work [4–7, 9], in the setting of bluff body flow, we propose a method for the computation of mean value output in turbulent flow, based on adaptive computation of approximate weak solutions to the Navier–Stokes equations using stabilized finite element methods, which we here refer to as *General Galerkin (G2) methods*. In [4–7, 9] the no slip boundary condition is shown to accurately capture the separation from laminar boundary layers. In this paper we extend the G2 method to problems of turbulent boundary layers, by including a simple wall-model in the form of a friction boundary condition to account for the skin friction of the unresolved turbulent boundary layer. In particular, for a circular cylinder we consider the problem of drag crisis, and the limit of zero viscosity, corresponding to the Euler equations with slip boundary conditions.

The incompressible Navier–Stokes (NS) equations for a unit density Newtonian fluid with constant kinematic viscosity $\nu > 0$ enclosed in a volume $\Omega$ in $\mathbb{R}^3$ (where we assume that $\Omega$ is a polygonal domain), take the form:

$$R(\hat{u}) = 0, \quad \text{in } \Omega \times I, \tag{1}$$

for $\hat{u} = (u, p)$, with $u(x, t)$ the *velocity vector* and $p(x, t)$ the *pressure* at $(x, t)$, $I = (0, T)$ is a time interval, and $R(\hat{u}) \equiv \bar{R}(\hat{u}) - (f, 0) = (\bar{R}_1(\hat{u}), \bar{R}_2(u)) - (f, 0)$, with

$$\begin{aligned} \bar{R}_1(\hat{u}) &= \dot{u} + u \cdot \nabla u + \nabla p - \nu \Delta u, \\ \bar{R}_2(u) &= \nabla \cdot u, \end{aligned} \tag{2}$$

together with initial condition $u(x, 0) = u^0(x)$ and appropriate boundary conditions. The quantity $\nu \Delta u - \nabla p$ represents the total fluid force (modulo the external force $f$), and may alternatively be expressed as

$$\nu \Delta u - \nabla p = \nabla \cdot \sigma(\hat{u}), \tag{3}$$

where $\sigma(\hat{u}) = (\sigma_{ij}(\hat{u}))$ is the *stress tensor*, with components $\sigma_{ij}(\hat{u}) = 2\nu\epsilon_{ij}(u) - p\delta_{ij}$, composed of the *stress deviatoric* $2\nu\epsilon_{ij}(u)$ with zero trace and an isotropic pressure: here $\epsilon_{ij}(u) = (u_{i,j} + u_{j,i})/2$ is the *strain rate tensor*, with

J. Hoffman
School of Computer Science and Communication, Royal Institute of Technology KTH, 10044 Stockholm, Sweden
E-mail: jhoffman@csc.kth.se

$u_{i,j} = \partial u_i/\partial x_j$, and $\delta_{ij}$ is the usual Kronecker delta, the indices $i$ and $j$ ranging from 1 to 3.

A given flow may be characterized by the *Reynolds number* $Re = UL/\nu$, where $U$ and $L$ are representative velocity and length scales, respectively, and with $U$ and $L$ normalized to unity we have $Re = \nu^{-1}$. Setting the viscosity $\nu = 0$, corresponds to the Euler equations with $Re = \infty$. For $Re$ sufficiently large we expect to have a partly turbulent flow, and to resolve all the physical scales in a turbulent flow, one may estimate the number of mesh points needed to be of the order $Re^3$ in space-time [3]. In many applications of industrial importance we have $Re > 10^6$, and thus a Direct numerical simulation (DNS) of the NS equations is impossible.

The traditional approach to get around the impossibility of DNS at higher Reynolds numbers is to apply an averaging operator to the NS equations, to obtain a new set of equations for the averaged flow variables. This is, for example, the approach taken in a large eddy simulation (LES), where the averaging operator typically is a spatial filter, removing the finest scales of the solution. Filtering of the non linear term in the NS equations leads to the introduction of so called *Reynolds stresses* (or *LES stresses*), which depend on the unfiltered velocity field, and thus need to be modelled in terms of the filtered velocity in a *turbulence model* (or *subgrid model*), which is referred to as the problem of *closure*. Many subgrid models have been proposed, typically having a dissipative nature, and we refer to [21] for an overview of LES and subgrid modeling. It seems fair to say that the closure problem is still unsolved, with existing subgrid models being problem dependent, and highly sensitive to the numerical method used in the simulation. Finding boundary conditions, or *wall models*, for LES is also a very active field of research, see [21].

In [8] we propose a framework for the study of existence and uniqueness of solutions to the NS equations based on approximate weak solutions, which we refer to as *$\epsilon$-weak solutions*. Existence is given by construction using a G2 method to compute an approximate weak solution, for which uniqueness in output (or *weak uniqueness*) is studied by computing an approximation of an associated dual problem linearized at the G2 solution and with data coupling to the output.

For turbulent flow we sometimes refer to an adaptive G2 method as *Adaptive DNS/LES*, where adaptively some critical parts of the flow are resolved in a DNS, whereas other parts are left underresolved in a LES. Adaptive DNS/LES is presented in [5, 9] as a general method for the computation of mean value output in turbulent flow. The adaptive method is based on a posteriori error estimates, where a linearized dual problem is solved computationally to determine the sensitivity of a certain output with respect to discretization errors and modeling errors from unresolved scales in the turbulent flow. In [5, 9] it is shown that with G2 it is possible to compute correct mean value output, such as drag and lift, using a rather coarse mesh with the number of degrees of freedom being orders of magnitude less than for standard LES methods in the literature.

In [5, 9], only the flow past bluff bodies with square geometries is investigated, a square cylinder and a surface mounted cube, for which the separation of the flow is given by the geometry. For rounded geometries this is not the case, instead the position of the separation points (lines) depend on the Reynolds number, which is the case in [6, 7], where a circular cylinder and a sphere are investigated. For any section of the cylinder or the midsection of the sphere, we define an angle $\theta$ starting from the upstream stagnation point. From the upstream stagnation point, where the pressure is very high, the flow accelerates and the pressure near the boundary is decreasing up to $\theta \approx 90°$, where the pressure starts to increase again, which results in an adverse pressure gradient acting as a negative force in the momentum equation. If the momentum close to the boundary is too low, the adverse pressure gradient will force the flow to separate. For $Re \sim 10^3 - 10^5$ separation will occur close to $\theta = 90°$, leading to a large turbulent wake and a drag coefficient $c_D \approx 1.0$ for the cylinder, and $c_D \approx 0.40$ for the sphere. In [6, 7] these and other mean quantities are well predicted using G2 and no slip boundary conditions, again using very few degrees of freedom.

Increasing the Reynolds number further, the laminar boundary layer will undergo transition to turbulence. A turbulent boundary layer has a sharp mean velocity profile, with higher momentum close to the boundary than for a laminar boundary layer. This increase in momentum near the boundary leads to a delayed separation of the boundary layer, with a smaller wake and lower drag as a result, so called *drag crisis*.

The momentum loss in the boundary layer couples to *skin friction*, which is decreasing with higher Reynolds numbers. For higher Reynolds numbers the momentum near the boundary increases, and the separation is delayed. To resolve the boundary layer computationally at these high Reynolds numbers would be very expensive, and in this paper we propose to instead use a simple approach where the boundary condition is directly coupled to skin friction, using a *slip with friction boundary condition*, a type of boundary condition considered already by Navier [19] and Maxwell [16]. This type of boundary condition has earlier been studied e.g. in [10–13], in the setting of near wall models for LES, where analytical forms of the friction coefficient are derived for some special flow cases based on boundary layer theory, and numerical tests are performed for the low Reynolds number flow around a square cylinder in 2d and 3d. In this paper we use a slip with friction boundary condition to model turbulent boundary layers for very high Reynolds numbers.

In particular, we find that for the case $Re \to \infty$, corresponding to an Euler solution with skin friction $\to 0$, the separation points for the circular cylinder move downstream to eventually collapse into one single separation point, resulting in a solution resembling the potential solution with a very low drag. Although, this solution is not stable, and the single separation point (line) generates vorticity and starts to oscillate. The generation of vorticity along the separation line leads to turbulence behind the cylinder, although the separation is still concentrated in one single separation point

(in each spanwise section of the cylinder). Also, structures similar to a regular von Karman vortex shedding appear, with the difference that for the Euler solution *there is only one separation point*, rather than the two separation points appearing in the low Reynolds number flow, and there is a strong variation in the position of the separation point along the cylinder.

We refer to such a solution with $\nu = 0$ and slip boundary conditions as an *Euler/G2 (EG2) solution*, in which the only parameter left in the model is the discretization parameter $h$. That is, no empirical constants or modeling parameters. We expect that some mean value output may be independent of $h$, in which case EG2 is a truly parameter-free model with respect to such output.

The question is then if such an EG2 solution is to be found in Nature? There is no experimental data avaliable for the cylinder above $Re = 10^7$, and increasing the velocity eventually makes the incompressible flow model invalid. The other parameter determining the Reynolds number (restricting ourselves to the viscosity of air or water) is the length scale, leading us to seek the EG2 solution for flow phenomena with very large length scales. Indeed, studying geophysical bluff body problems [18] it seems clear that the separation is taking place in one point, rather that in two points with a wake in between as for the low Reynolds number solution. We expect that in such problems of very large length scales, the EG2 model may prove to be important.

We note that using G2 with low friction at the boundary is very cheap computationally, since there is no boundary layer to resolve.

In this paper we first recall the definition of an $\epsilon$-weak solution to the NS equations, weak uniqueness, and a G2 method for the approximation of the drag of a bluff body. This is important for the presentation to make clear what type of solution we seek to approximate: using G2 we compute approximate weak solutions to the NS equations, as opposed to LES where one seeks to approximate a filtered solution to the NS equations. We then recall some results for bluff body flow with laminar separation, which we extend to turbulent separation using slip with friction boundary conditions, modeling drag crisis with small friction and EG2 solutions with pure slip conditions.

## 2 $\epsilon$-Weak solutions to the Navier–Stokes equations

To study weak uniqueness of the NS equations we introduce in [8] the concept of an *$\epsilon$-weak solution*, which is an approximate weak solution with a residual less than $\epsilon$ in a weak norm. We define for $\hat v = (v, q) \in \hat V$,

$$((R(\hat u), \hat v)) \equiv ((\dot u, v)) + ((u \cdot \nabla u, v)) - ((\nabla \cdot v, p)) + ((\nabla \cdot u, q)) + ((2\nu\epsilon(u), \epsilon(v))) - ((f, v)), \quad (4)$$

where

$$\hat V = \{\hat v = (v, q) \in H^1(Q)^4 : v \in L_2(I; H_0^1(\Omega)^3)\},$$

and $((\cdot, \cdot))$ is the $L_2(Q)^m$ inner product with $m = 1, 3$, or a suitable duality pairing, over the space-time domain $Q = \Omega \times I$, where $H_0^1(\Omega)$ is the usual Sobolev space of functions being zero on the boundary $\Gamma$ and square integrable together with their first derivatives over $\Omega$, with dual $H^{-1}(\Omega)$. As usual, $L_2(I; X)$ with $X$ a Hilbert space denotes the set of functions $v : I \to X$ which are square integrable.

We now define $\hat u \in \hat V$ to be an $\epsilon$-weak solution if

$$|((R(\hat u), \hat v))| \le \epsilon \|\hat v\|_{\hat V}, \quad \forall \hat v \in \hat V, \quad (5)$$

where $\|\cdot\|_{\hat V}$ denotes the $H^1(Q)^4$-norm, and we define $\hat W_\epsilon$ to be the set of $\epsilon$-weak solutions for a given $\epsilon > 0$. Note that for simplicity we here ask also the solution $\hat u$ to belong to the test space $\hat V$, which require more regularity than necessary; for the formulation (5) to make sense, it is sufficient that $R(\hat u)$ belongs the dual space of $\hat V$, so that (4) is well defined. Equivalently, we may say that $\hat u \in \hat V$ is an $\epsilon$-weak solution if

$$\|R(\hat u)\|_{\hat V'} \le \epsilon,$$

where $\|\cdot\|_{\hat V'}$ is the dual norm to the norm of $\hat V$. This is a weak norm measuring mean values of $R(\hat u)$ with decreasing weight as the size of the mean value decreases. Pointvalues are thus measured very lightly.

## 3 Output sensitivity and the dual problem

Suppose now the *quantity of interest*, or *output*, related to a given $\epsilon$-weak solution $\hat u$ is a scalar quantity of the form

$$M(\hat u) = ((\hat u, \hat\psi)), \quad (6)$$

which represents a mean-value in space-time, where $\hat\psi = (\psi_1, \psi_2) \in L_2(\Omega)^3 \times L_2(\Omega)$ is a given weight function. In typical applications the output could be a drag or lift coefficient in a bluff body problem. In this case the weight $\hat\psi$ is a piecewise constant in space-time. More generally, $\hat\psi$ may be a piecewise smooth function corresponding to a mean-value output.

We now seek to estimate the difference in output of two different $\epsilon$-weak solutions $\hat u = (u, p)$ and $\hat w = (w, r)$. We thus seek to estimate a certain form of *output sensitivity* of the space $\hat W_\epsilon$ of $\epsilon$-weak solutions. To this end, we introduce the following linearized dual problem of finding $\hat\varphi = (\varphi, \theta) \in \hat V$, such that

$$a(\hat u, \hat w; \hat v, \hat\varphi) = ((\hat v, \hat\psi)), \quad \forall \hat v \in \hat V_0, \quad (7)$$

where $\hat V_0 = \{\hat v \in \hat V : v(\cdot, 0) = 0\}$, and

$$a(\hat u, \hat w; \hat v, \hat\varphi) \equiv ((\dot v, \varphi)) + ((u \cdot \nabla v, \varphi)) + ((v \cdot \nabla w, \varphi)) + ((\nabla \cdot \varphi, q)) - ((\nabla \cdot v, \theta)) + ((2\nu\epsilon(v), \epsilon(\varphi)))$$

with $u$ and $w$ acting as coefficients, and $\hat\psi$ is given data.

This is a linear convection–diffusion-reaction problem in variational form, $u$ acting as the convection coefficient and $\nabla w$ as the reaction coefficient, and the time variable runs "backwards" in time with initial value ($\varphi(\cdot, T) = 0$) given

at final time $T$ imposed by the variational formulation. The reaction coefficient $\nabla w$ may be large and highly fluctuating, and the convection velocity $u$ may also be fluctuating.

Choosing now $\hat{v} = \hat{u} - \hat{w}$ in (7), we obtain

$$M(\hat{u}) - M(\hat{w}) = a(\hat{u}, \hat{w}; \hat{u} - \hat{w}, \hat{\varphi}) = ((R(\hat{u}), \hat{\varphi})) - ((R(\hat{w}), \hat{\varphi})), \quad (8)$$

and thus we may estimate the difference in output as follows:

$$|M(\hat{u}) - M(\hat{w})| \le 2\epsilon \|\hat{\varphi}\|_{\hat{V}}. \quad (9)$$

By defining the *stability factor* $S(\hat{u}, \hat{w}; \hat{\psi}) = \|\hat{\varphi}\|_{\hat{V}}$, we can write

$$|M(\hat{u}) - M(\hat{w})| \le 2\epsilon S(\hat{u}, \hat{w}; \hat{\psi}), \quad (10)$$

and by defining

$$S_\epsilon(\hat{\psi}) = \sup_{\hat{u}, \hat{w} \in \hat{W}_\epsilon} S(\hat{u}, \hat{w}; \hat{\psi}), \quad (11)$$

we get

$$|M(\hat{u}) - M(\hat{w})| \le 2\epsilon S_\epsilon(\hat{\psi}), \quad (12)$$

which expresses output uniqueness of $\hat{W}_\epsilon$. Depending on $\hat{\psi}$, the stability factor $S_\epsilon(\hat{\psi})$ may be small, medium, or large, reflecting different levels of output sensitivity, where we expect $S_\epsilon(\hat{\psi})$ to increase as the mean value becomes more local. The concept of weak uniqueness is presented in detail in [8].

## 4 General Galerkin G2

To generate approximate weak solutions we use a stabilized finite element method of the form: find $\hat{U} \equiv \hat{U}_h \in \hat{V}_h$, where $\hat{V}_h \subset \hat{V}$ is a finite dimensional subspace defined on a computational mesh in space-time of mesh size $h$, such that

$$((R(\hat{U}), \hat{v})) + ((\delta R(\hat{U}), \bar{R}(\hat{v}))) = 0, \quad \forall \hat{v} \in \hat{V}_h, \quad (13)$$

where $\delta = \delta(h, \hat{U})$ is a stabilization parameter, and the residual is defined by $R(\hat{U}) \equiv \bar{R}(\hat{U}) - (f, 0) = (\bar{R}_1(\hat{U}), \bar{R}_2(U)) - (f, 0)$, such that for $\hat{w} = (w, r)$,

$$\begin{aligned} \bar{R}_1(\hat{w}) &= \dot{w} + U \cdot \nabla w + \nabla r - \nu \Delta w, \\ \bar{R}_2(w) &= \nabla \cdot w, \end{aligned} \quad (14)$$

with elementwise definition of second order terms. We here interpret a convection term $((U \cdot \nabla w, v))$ as

$$\frac{1}{2}((U \cdot \nabla w, v)) - \frac{1}{2}((U \cdot \nabla v, w),$$

which is literally true if $\nabla \cdot U = 0$. With this interpretation we will have $((U \cdot \nabla U, U)) = 0$, even if the divergence of the finite element velocity $U$ does not vanish exactly. Choosing $\hat{v} = \hat{U}$ in (13), and assuming that $f = 0$, we obtain the following energy balance:

$$\frac{1}{2}\|U(T)\|^2 + ((\nu \nabla U, \nabla U)) + ((\delta R(\hat{U}), R(\hat{U}))) = \frac{1}{2}\|u^0\|^2. \quad (15)$$

The finite element method (13) is a stabilized Galerkin method with the term $((R(\hat{U}), v))$ corresponding to Galerkin's method and the term $((\delta R(\hat{u}), \bar{R}(\hat{v})))$ corresponding to a weighted residual least squares method with stabilizing effect expressed in (15). We also refer to this method as *G2* or *General Galerkin*, and we thus refer to $\hat{U}$ as a *G2 solution*. In [8] we prove that a G2 solution $\hat{U}$ is also an $\epsilon$-weak solution with $\epsilon = C_U \|hR(\hat{U})\|$, with $C_U$ a constant, assuming that the maximum of the computed velocity is bounded (or grows slower than $h^{-1/2}$).

With $\nu = 0$ we have a G2 method for the Euler equations, which we refer to as an *Euler/G2 solution*, or an *EG2 solution*. For an EG2 solution the least squares term is the only stabilizing term in the method, and the only parameter in the method is the discretization parameter $h$.

## 5 Computability and a posteriori error estimation for G2

We now let $\hat{u}$ be an $\epsilon$-weak solution of the NS equations with $\epsilon$ small, and we let $\hat{U}$ be a G2 solution, which can be viewed to be an $\epsilon_{G2}$-weak solution, with $\epsilon_{G2} = C_U \|hR(\hat{U})\| >> \epsilon$. As in (12), we get the following a posteriori error estimate for a mean value output given by a function $\hat{\psi}$:

$$|M(\hat{u}) - M(\hat{U})| \le (C_U \|hR(\hat{U})\| + \epsilon) S_{\epsilon_{G2}}(\hat{\psi}), \quad (16)$$

where $S_{\epsilon_{G2}}(\hat{\psi})$ is the corresponding stability factor defined by (11). Obviously the size of the stability factor $S_{\epsilon_{G2}}(\hat{\psi})$ is crucial for computability.

We note that for weak uniqueness the residual only needs to be small in a weak norm, and correspondingly for computability the G2 residual only needs to be small when weighted by $h$. This means that for accurate approximation of a mean value output, the NS equations do not need to be satisfied pointwise, corresponding to a pointwise small residual, but only in an average sense, corresponding to the residual being small only in a weak norm. In computations we find that in fact the G2 residual in a turbulent flow typically is large pointwise, also for solutions corresponding to accurate approximation of mean value output, such as the drag of a bluff body.

## 6 The cG(1)cG(1) method

The cG(1)cG(1) method is a variant of G2 using the continuous Galerkin method cG(1) in space and time. With cG(1) in time the trial functions are continuous piecewise linear and the test functions piecewise constant. cG(1) in space corresponds to both test functions and trial functions being continuous piecewise linear. Let $0 = t_0 < t_1 < \ldots < t_N = T$ be a sequence of discrete time steps with associated time intervals $I_n = (t_{n-1},\ t_n]$ of length $k_n = t_n - t_{n-1}$ and space-time slabs $S_n = \Omega \times I_n$, and let $W^n \subset H^1(\Omega)$ be a finite element space consisting of continuous piecewise linear functions on a mesh $\mathcal{T}_n = \{K\}$ of mesh size $h_n(x)$ with $W^n_w$ the functions $v \in W^n$ satisfying the Dirichlet boundary condition $v|_{\partial\Omega} = w$.

We now seek functions $\hat{U} = (U, P)$, continuous piecewise linear in space and time, and the cG(1)cG(1) method for the Navier–Stokes equations (1), with homogeneous Dirichlet boundary conditions reads: For $n = 1, \ldots, N$, find $(U^n, P^n) \equiv (U(t_n), P(t_n))$ with $U^n \in V_0^n \equiv [W_0^n]^3$ and $P^n \in W^n$, such that

$$
\begin{aligned}
&((U^n - U^{n-1})k_n^{-1} + \hat{U}^n \cdot \nabla \hat{U}^n, v) + (2\nu\epsilon(\hat{U}^n), \epsilon(v)) \\
&-(P^n, \nabla \cdot v) + (\nabla \cdot \hat{U}^n, q) + SD_\delta(\hat{U}^n, P^n; v, q) \\
&= (f, v) \quad \forall (v, q) \in V_0^n \times W^n, \qquad (17)
\end{aligned}
$$

where $\hat{U}^n = \frac{1}{2}(U^n + U^{n-1})$, with the stabilizing term

$$
\begin{aligned}
&SD_\delta(\hat{U}^n, P^n; v, q) \\
&\quad \equiv (\delta_1(\hat{U}^n \cdot \nabla \hat{U}^n + \nabla P^n - f), \hat{U}^n \cdot \nabla v + \nabla q) \\
&\qquad + (\delta_2 \nabla \cdot \hat{U}^n, \nabla \cdot v),
\end{aligned}
$$

with $\delta_1 = 1/2(k_n^{-2} + |U|^2 h_n^{-2})^{-1/2}$ in the convection-dominated case $\nu < \bar{U}^n h_n$ and $\delta_1 = \kappa_1 h_n^2$ otherwise, $\delta_2 = \kappa_2 h_n$ if $\nu < \bar{U}^n h_n$ and $\delta_2 = \kappa_2 h_n^2$ otherwise, with $\kappa_1$ and $\kappa_2$ positive constants of unit size (in this paper we have $\kappa_1 = \kappa_2 = 1$), and

$$
(v, w) = \sum_{K \in \mathcal{T}_\backslash} \int_K v \cdot w \, \mathrm{d}x,
$$

$$
(\epsilon(v), \epsilon(w)) = \sum_{i,j=1}^{3} (\epsilon_{ij}(v), \epsilon_{ij}(w)).
$$

We note that the time step $k_n$ is given by the mesh size $h_n$, with typically $k_n \sim h_n$.

## 7 Slip with friction boundary conditions

The *slip with friction and penetration with resistance boundary condition* for a boundary $\Gamma_{slfr}$ with normal $n$ and two orthogonal tangential vectors $\tau_1, \tau_2$ takes the form

$$
u \cdot n + \alpha \, n^T \sigma n = 0, \qquad (18)
$$

$$
u \cdot \tau_k + \beta^{-1} n^T \sigma \tau_k = 0, \quad k = 1, 2, \qquad (19)
$$

with the stress tensor $\sigma = \sigma(\hat{u})$, and where we use matrix notation with all vectors $v$ being column vectors and the corresponding row vector is denoted $v^T$.

Here $\alpha$ is a penetration parameter and $\beta$ is a friction parameter, both positive functions defined on the boundary. In principle, $(\alpha, \beta) \to (0, \infty)$ corresponds to a penalty imposition of a no slip boundary condition, and $(\alpha, \beta) \to (0, 0)$ corresponds to a penalty imposition of a slip boundary condition. By increasing $\beta$ we increase the resistance at the boundary, and by increasing $\alpha$ we increase the penetration of the boundary.

We can implement (18), (19) weakly by decomposing the test function $v$ into components aligned with the normal and tangent directions:

$$
v = (v \cdot n)n + \sum_{k=1}^{2} (v \cdot \tau_k)\tau_k, \qquad (20)
$$

see e.g. [11] for an algorithm for determining two linearly independent tangent vectors. We then have

$$
\begin{aligned}
\int_{\Gamma_{slfr}} (\sigma \cdot n) \cdot v \, \mathrm{d}s &= \int_{\Gamma_{slfr}} n^T \sigma n (v \cdot n) \\
&\quad + \sum_{k=1}^{2} n^T \sigma \tau_k (v \cdot \tau_k) \, \mathrm{d}s \\
&= -\int_{\Gamma_{slfr}} \alpha^{-1} (u \cdot n)(v \cdot n) \\
&\quad - \sum_{k=1}^{2} \beta (u \cdot \tau_k)(v \cdot \tau_k) \, \mathrm{d}s. \qquad (21)
\end{aligned}
$$

The derivation of the weak formulation of Eq. (1) underlying the cG(1)cG(1) method Eq. (17) formally involves partial integration of Eq. (1), resulting in the term

$$
(2\nu\epsilon(U^n), \epsilon(v)) - (P^n, \nabla \cdot v) = (\sigma(U^n, P^n), \epsilon(v)), \qquad (22)
$$

in the left hand side of Eq. (17), together with a surface integral

$$
\int_{\Gamma_{slfr}} (\sigma(U^n, P^n) \cdot n) \cdot v \, \mathrm{d}s. \qquad (23)
$$

This surface integral is zero in Eq. (17), since the test function $v \in V_0^n$ satisfies a homogeneous Dirichlet condition.

To implement the boundary conditions (18), (19), we seek a solution $(U^n, P^n) \in [W^n]^3 \times W^n$ for $n = 1, ..., N$, satisfying Eq. (17) for $(v, q) \in [W^n]^3 \times W^n$, with the surface integral (23) subtracted from the left hand side of (17). Substituting the surface integral by (21) then corresponds to a weak implementation of the boundary conditions (18), (19). We here assume that there exists a unique solution to this problem.

We stress that one has to be careful when implementing this boundary condition; one needs to use normals and tangent vectors that are defined for each node in the mesh, not for each face (or edge in 2 dimensions). The reason is that in the case the boundary $\Gamma_{slfr}$ is not a flat surface, the degrees of freedom in certain nodes will be forced to satisfy conditions in too many directions. For example, in the case of a slip condition with $(\alpha, \beta) = (0, 0)$, the degrees of freedom in a node will be forced to satisfy a non penetration condition in several linearly independent directions, which may result instead in a no slip boundary condition.

By choosing $\hat{v} = \hat{U}$ in (17), we note that (21) corresponds to penalty terms for the $L_2$-norms of the normal and tangential components of the velocity at the boundary, with penalty parameters $\alpha^{-1}$ and $\beta$, and that the energy balance (15) is modified by adding the time integrals of the terms

$$
\|\alpha^{-1/2} u \cdot n\|_{\Gamma_{slfr}} + \sum_{k=1}^{2} \|\beta^{1/2} u \cdot \tau_k\|_{\Gamma_{slfr}} \qquad (24)
$$

to the left hand side of Eq. (15).

## 8 Adaptive algorithm

A mean value in time of the force on a body, over a time interval $I$, may be expressed as [5]:

$$N(\sigma(\hat{u})) = \frac{1}{|I|}\int_I (\dot{u} + u\cdot\nabla u - f, \Phi) - (p, \nabla\cdot\Phi) + (2\nu\epsilon(u), \epsilon(\Phi)) + (\nabla\cdot u, \Theta)\,\mathrm{d}t, \quad (25)$$

where $\hat{u}$ is an $\epsilon$-weak solution to the NS equations, and $\Phi$ is a function defined in the fluid volume $\Omega$ being equal to a unit vector in the direction of the force we want to compute on $\Gamma_0$, the surface of the body in contact with the fluid, and zero on the remaining part of the boundary $\Gamma_1 = \partial\Omega \setminus \Gamma_0$. The representation (25) is independent of $\Theta$, and the particular extension of $\Phi$ away from the boundary, and we ask that $\hat{\Phi} = (\Phi, \Theta) \in \hat{V}$.

We compute an approximation of the drag $N(\sigma(\hat{u}))$ from a cG(1)cG(1) solution $\hat{U}$, using the formula

$$N^h(\sigma(\hat{U})) = \frac{1}{|I|}\int_I (\dot{U} + U\cdot\nabla U - f, \Phi) - (P, \nabla\cdot\Phi) + (2\nu\epsilon(U), \epsilon(\Phi)) + (\nabla\cdot U, \Theta) + SD_\delta(U, P; \Phi, \Theta)\,\mathrm{d}t, \quad (26)$$

where now $\Phi$ and $\Theta$ are finite element functions, and where $\dot{U} = (U^n - U^{n-1})/k_n$ on $I_n$. We note the presence of the stabilizing term $SD_\delta$ in (26) compared to Eq. (25), which is added in order to obtain the independence of $N^h(\sigma(\hat{U}))$ from the choice of $(\Phi, \Theta)$, given by Eq. (17).

Approximating $\hat{\varphi} = (\varphi, \theta)$, the exact solution to the dual problem (7), by a computed approximation $\hat{\varphi}_h = (\varphi_h, \theta_h)$, with the linearized convection velocity $u \approx U$, we are led to the following a posteriori error estimate [5] for the time average over $I$ of the drag force on a body in a fluid, with respect to $\hat{u} \in W_\epsilon$:

$$|N(\sigma(\hat{u})) - N^h(\sigma(\hat{U}))| \approx \epsilon S_\epsilon(\hat{\psi}) + \sum_{K\in\mathcal{T}_n} \mathcal{E}_{K,h}, \quad (27)$$

where $\hat{\psi} = (\Phi, 0)$ is the data to the dual problem defining the output $N(\sigma(\cdot))$, $k$ and $h$ are the time step and the local mesh size, respectively, and $\mathcal{E}_{K,h} = e^K_{D,h} + e^K_{M,h}$, with

$$e^K_{D,h} = \frac{1}{|I|}\int_I \big((|R_1(\hat{U})|_K + |R_2(\hat{U})|_K) \cdot (C_h h^2 |D^2\varphi_h|_K + C_k k|\dot{\varphi}_h|_K) + \|R_3(\hat{U})\|_K \cdot (C_h h^2 \|D^2\theta_h\|_K + C_k k\|\dot{\theta}_h\|_K)\big)\,\mathrm{d}t,$$

$$e^K_{M,h} = \frac{1}{|I|}\int_I SD_\delta(\hat{U}; \hat{\varphi}_h)_K\,\mathrm{d}t,$$

where we may view $e^K_{D,h}$ as the error contribution from the Galerkin discretization in cG(1)cG(1), and $e^K_{M,h}$ as the contribution from the stabilization in cG(1)cG(1), on element $K$. The lower bound on the tolerance, defining computability of the output $N(\sigma(\cdot))$, is given by $\epsilon S_\epsilon(\hat{\psi})$. Here we think of $\epsilon$ as being small, corresponding to a maximal computational cost, so that $\epsilon S_\epsilon(\hat{\psi}) << \sum_{K\in\mathcal{T}_n} \mathcal{E}_{K,h}$.

We now present an algorithm for adaptive mesh refinement based on the a posteriori output error estimate (27). For simplicity, we here use the same space mesh for all time steps.

**Algorithm 1 (Adaptive mesh refinement)** *Given an initial coarse computational space mesh $\mathcal{T}^0$, start at $k = 0$, then do*

*(a) Compute approximation of the primal problem using $\mathcal{T}^k$.*
*(b) Compute approximation of the dual problem using $\mathcal{T}^k$.*
*(c) If $|\sum_{K\in\mathcal{T}_k} \mathcal{E}^k_{K,h}| < TOL$ then STOP, else:*
*(d) Based on the size of the local error indicator $\mathcal{E}^k_{K,h}$, mark a fixed fraction of the elements in $\mathcal{T}^k$ for refinement. Obtain a new refined mesh $\mathcal{T}^{k+1}$, using a standard algorithm for local mesh refinement.*
*(e) Set $k = k + 1$, then goto (a).*

## 9 Drag crisis

The drag of a bluff body may be divided into pressure drag, coupling to the pressure drop over the body, and skin friction. Separation of the flow influence the relation between pressure drag and skin friction, with typically an earlier separation leading to higher pressure drag and lower skin friction.

For square geometries the separation is given by the geometry, see e.g. [5, 14, 20], whereas for the flow past a circular geometry, the separation is not given by the geometry, but depend on the Reynolds number, see e.g. [1, 6, 7, 15, 17, 22, 23].

For a circular geometry, such as a circular cylinder or a sphere, the flow does not separate at all for very low Reynolds numbers, where the skin friction dominates the contribution to the total drag, and then for increasing Reynolds numbers the wake increases and the separation points (lines) move upstream until reaching $\theta \approx 90°$, with $\theta$ an angle in the circular section counted from zero at the upstream stagnation point. In this configuration pressure drag is dominating skin friction, and the total drag is more or less constant ($c_D \approx 1.0$ for a circular cylinder and $c_D \approx 0.4$ for a sphere) for a wide range of Reynolds numbers ($Re \approx 10^3 - 10^5$).

In [6, 7], the drag of a circular cylinder and a sphere is computed using G2, with accurate approximation of drag using no slip boundary conditions and very coarse meshes (of the order $10^5$ mesh points).

At very high Reynolds numbers ($Re \approx 10^5 - 10^6$) the boundary layer for a circular cylinder and a sphere undergoes transition to turbulence, making the separation points (lines) move downstream as the Reynolds number increases, resulting in a smaller wake and lower drag, so called *drag crisis*. Simulation of drag crisis is a major challenge of turbulence simulation.

## Simulation of drag crisis

To resolve the very thin boundary layer of a high Reynolds number flow is too expensive, and thus many different wall-models have been proposed to capture the effect of the boundary layer without resolving it to its physical scale, see [21] for an overview. In [2] a Detached-eddy simulation is used to simulate drag crisis for a sphere. A Detached-eddy simulation is a hybrid approach that has the behaviour of a RANS model near the boundary and becomes a LES in the regions away from solid surfaces, see [21].

In this paper we propose a simple approach to model the effect of the boundary layer, based on a slip with friction boundary condition, which may be viewed as a very simple wall-model. The idea is that the main effect of the boundary layer on the flow is skin friction. The problem is then to choose a suitable friction coefficient $\beta$.

In [10–13], similar boundary conditions are used to study reattachement of a low Reynolds number flow past a surface mounted cube in 2d and 3d as a function of the friction parameter $\beta$, and it is found that reattachement is delayed with decreasig friction, as expected.

For very high Reynolds numbers the viscous $\nu$-term in the computational method (17) is neglible if we do not resolve the finest scales of the flow, and may be dropped from the equation, corresponding to a cG(1)cG(1) method for the Euler equations. The energy dissipation in the flow is then only due to the boundary conditions and the stabilizing term in (17), which is expressed in the energy balance (15) with (24) (setting $\alpha = 0$):

$$\tfrac{1}{2}\|U(T)\|^2 + ((\delta R(\hat{U}), R(\hat{U}))) + \int_0^T \sum_{k=1}^{2} \|\beta^{1/2} u \cdot \tau_k\|_{\Gamma_{slfr}} \,\mathrm{d}t = \frac{1}{2}\|u^0\|^2, \tag{28}$$

recalling that $((\cdot,\cdot))$ implies integration in space-time.

The dissipation is a characteristic feature of the turbulent flow, and in [5] we find that for the flow past a square cylinder and a surface mounted cube the dissipation in the turbulent wake is independent of $h$ after some refinement of the mesh. This indicates that to capture the correct mean dissipation of the wake we do not have to further resolve the flow in the wake once we have reached a certain $h$, which also couples to the basic empirical *Law of finite energy dissipation* [3]. The results in [4–7, 9] indicate that the correct mean dissipation of the wake is captured on rather coarse meshes, and that the degree of resolution needed is determined automatically by the adaptive algorithm.

A main computational challenge is to capture the correct separation of the flow and the correct dissipation in the boundary layer. Flow separation is determined by the momentum equation, where an adverse pressure gradient in the flow direction corresponds to a force in the opposite direction which reduces the momentum. When this retarding force has reduced the momentum to zero near the boundary the flow separates. High skin friction corresponds to a low Reynolds number and a laminar boundary layer with low momentum near the boundary, whereas low skin friction corresponds to a high Reynolds number and a turbulent boundary layer with high momentum near the boundary. Thus high skin friction corresponds to an earlier separation, and conversely when the skin friction decreases with the Reynolds number, the separation is delayed since the momentum near the boundary increases.

The idea underlying the boundary layer model in this paper is that for flow separation, the important characteristic of the boundary layer is the momentum near the boundary, which in turn depends of the skin friction at the boundary. Thus we should be able to capture the correct separation of a boundary layer as long as we have correct skin friction. We expect that $\beta \to 0$ for $Re \to \infty$, and we also expect $\beta$ to depend on the mesh resolution $h$, with $\beta \to \infty$ as $h \to 0$.

For the problems in [4–7, 9] the flow separates from a laminar boundary layer, corresponding to a relatively low Reynolds number, where it is possible to capture the separation using no slip boundary conditions (corresponding to $\beta = \infty$).

The criterion for choosing $\beta$ should be that the skin friction in the computation should be the same as in the physical problem. Experimental results [22] indicate that skin friction has a very weak dependence on the Reynolds number, proportional to $Re^{-0.2}$ in the case of a flat plate, and thus a certain value for $\beta$ should be characteristic for a rather wide range of Reynolds numbers. Experimental results [22] also indicate that once we have drag crisis the separation is again rather stable for a range of Reynolds numbers. The exact Reynolds number for when the separation point starts to move downstream seems to be hard to determine, which is probably due to its relation to the transition to turbulence in the laminar boundary layers, which in turn depends on the level of perturbations in the boundary layer, which is very hard to determine in a realistic problem. Thus, there is a range of Reynolds numbers, close to where transition in the boundary layers occur, for which the separation of the flow is very hard to determine. From an engineering point of view it is then important to take both the sub-critical and the super-critical scenario into account.

## Drag crisis for a circular cylinder

We now turn to the issue of modeling drag crisis for a circular cylinder of diameter $D$ and length $4D$, with the cylinder in the direction of the $x_3$-axis, subject to a unit streamwise velocity inflow condition (in the $x_1$-direction) in a channel of length $21D$, width $4D$, and height $14D$. We use slip boundary conditions on the lateral walls of the channel, and at the end of the channel we use a so called *transparant outflow boundary condition*, approximately corresponding to setting the stress to zero at the outflow boundary, see [8].

The *drag coefficient* $c_D$ is defined as a global average of a normalized drag force on an object from the fluid. We seek to approximate the drag coefficient $c_\mathrm{D}$ by $\bar{c}_\mathrm{D}$, a normalized drag force averaged over a finite time interval $I = [0, T]$, at

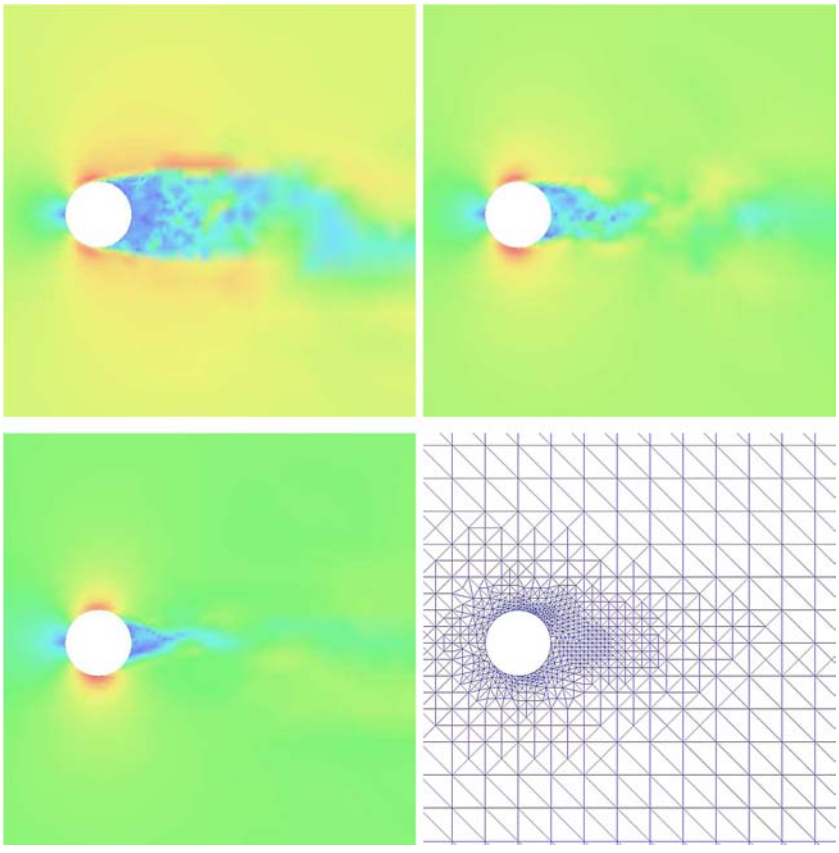

**Fig. 1** Drag crisis: magnitude of the velocity for G2 solutions for $\nu = 0$; $\beta = 2 \times 10^{-2}$ with $c_{\rm D} \approx 0.7$ (*upper left*), $\beta = 1 \times 10^{-2}$ with $c_{\rm D} \approx 0.5$ (*upper right*), $\beta = 5 \times 10^{-3}$ with $c_{\rm D} \approx 0.45$ (*lower left*), and the mesh with 80,000 mesh points (*lower right*), in the $x_1x_2$-plane for $x_3 = 0.2$

fully developed flow, defined by

$$\bar{c}_{\rm D} \equiv \frac{1}{(1/2)U_\infty^2 A} \times N(\sigma(\hat{u})), \tag{29}$$

where $U_\infty = 1$ is a reference velocity, $A$ is the projected area of the object facing the flow, and $N(\sigma(\hat{u}))$ is defined by Eq. (25) with $\Phi$ in the direction of the mean flow. In computations we approximate $\bar{c}_{\rm D}$ by $\bar{c}_{\rm D}^h$, defined by

$$\bar{c}_{\rm D}^h = \frac{1}{(1/2)U_\infty^2 A} \times N^h(\sigma(\hat{U})), \tag{30}$$

with $N^h(\sigma(\hat{U}))$ defined by Eq. (26). Thus we can use a scaled version of the a posteriori error estimate Eq. (27) to estimate the error $|\bar{c}_{\rm D} - \bar{c}_{\rm D}^h|$, upon which we base the adaptive algorithm.

Our model is here a cG(1)cG(1) method for the Euler equations together with a slip with friction boundary condition. Letting the friction parameter $\beta$ go from large to small values, we find that the separation point is moving downstream. For $\beta \approx 10^{-2}$ we find that we are able to capture the delayed separation of drag crisis with $c_{\rm D} \approx 0.4 - 0.5$, see Fig. 1. This value of $\beta$ is found by adjusting $\beta$ to match the experimental results.

## 10 Turbulent Euler solutions

> In a reasonable theory there are no dimensionless numbers whose values are only empirically determinable. (Einstein)

We now turn to the question of what happens as $\beta \to 0$, corresponding to the Reynolds number $Re \to \infty$. Our computational model then reduces to G2 for the Euler equations with slip boundary conditions, which we here refer to as an *Euler/G2 model*, or an *EG2 model*. We note that in this model the only parameter is the discretization parameter $h$.

### The dual problem for EG2

We recall that in computing the drag for a body, the mesh is refined using the a posteriori error estimate Eq. (27) based on a discrete approximation of the continuous dual problem Eq. (7), with unit boundary data for the dual velocity in the streamwise direction on the surface of the body.

The underlying error representation is based on the continuous dual problem, and thus we have to be careful so that the discrete (G2) approximation of the dual problem is a good enough approximation of the continuous dual problem. In [4–7, 9] we use no slip boundary conditions for the primal problem, and we find that after some mesh refinement the approximate dual weight in (27) is (approximately)

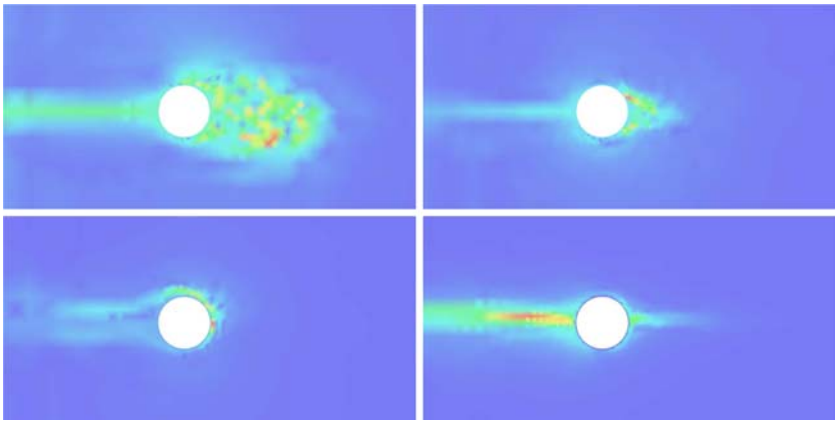

**Fig. 2** Magnitude of the dual velocity for $\beta = 0.1$ (*upper left*), $\beta = 0.01$ (*upper right*), and $\beta = 0$ (*lower left*), using velocity boundary data, and for $\beta = 0$ (*lower right*) using pressure data, in the $x_1x_2$-plane for $x_3 = 0.2$ (with 50, 000 nodes)

independent of the mesh refinement, which is taken as an indication of the validity of (27).

Since the normal component of the convection velocity field (the primal velocity) on the boundary in the dual problem is zero, the boundary data in the dual problem is only transported into the interior of the domain by diffusion. Although, with EG2 we have that $\nu = 0$, and thus it is not obvious how the boundary data is to be transported into the interior of the domain. In irregular parts of the flow, the stabilization will act as a numerical diffusion that will spread the data, but with the slip boundary condition in the primal problem the flow near the boundary will be smooth since there is no boundary layer, and thus the diffusion at the boundary will be very small.

With $\nu = 0$, the skin friction is zero and the mean drag $F_{\rm D}$ of a body with surface $\Gamma_0$ is solely due to the pressure:

$$F_{\rm D} = \frac{1}{|I|}\int_I \int_{\Gamma_0} pn_1 \, {\rm d}s \, {\rm d}t, \tag{31}$$

with $n_1$ the $x_1$-component of the normal.

For EG2, we propose to study instead the following quantity:

$$\tilde{F}_{\rm D} = \frac{1}{|I|}\frac{|\Gamma_0|}{|\tilde{\Gamma}_0|}\int_I \int_{\tilde{\Gamma}_0} p\tilde{n}_1 \, {\rm d}x \, {\rm d}t, \tag{32}$$

with $\tilde{n}_1$ a piecewise linear function in the finite element space $W^n$ which is equal to $n_1$ at all nodes on $\Gamma_0$ and zero at all other nodes. We define $\tilde{\Gamma}_0 \subset \Omega$ as the union of all cells in the mesh with at least one vertex on the surface $\Gamma_0$. The quantity $\tilde{F}_{\rm D}$ is then defined in (32) as a weighted average of the pressure $p$, which is of the same order of magnitude as $F_{\rm D}$. For example, for $\Gamma_0$ a straight line segment in 2d which is normal to the $x_1$-axis, piecewise linear approximation on uniform triangles, or bilinear approximation on uniform quadrilaterals, gives that $\tilde{F}_{\rm D} = 1/2\ F_{\rm D}$.

Formulating an adaptive method for the computation of $\tilde{F}_{\rm D}$ instead of $F_{\rm D}$ leads to the same a posteriori error estimate (27), but now with a different set of data for the dual problem. Instead of the boundary data for the dual velocity leading to an error representation for $F_{\rm D}$, we are now led to choose the data in the dual problem as a force in the dual continuity equation; that is we use homogeneous velocity boundary data, and the source term $\hat{\psi}$ in (7) we choose to be

$$\hat{\psi} = \left(0, \frac{|\Gamma_0|}{|\tilde{\Gamma}_0|}\,\tilde{n}_1\right). \tag{33}$$

With this data the issue of the missing boundary layer for $\nu = 0$ is avoided. Instead the data (33) establishes a pressure difference over the body in the dual problem, resulting (as expected) in a similar dual flow field as for the dual problems at lower Reynolds number with a boundary layer, see Fig. 2. Here we find that the dual solution with pressure data (33) to a large extent resembles the dual solutions for $\beta = 0.1, 0.01$ (modulo the different sizes of the turbulent wake), whereas the dual solution with velocity boundary data is not able to transport the boundary data into the interior of the domain, but only transports the data at the downstream separation point upstream.

We believe that for the approximation of pressure drag, the data (33) for the dual problem may be more appropriate also at lower Reynolds numbers, when the boundary layer is not fully resolved.

## EG2 for a circular cylinder

Experimental results for the circular cylinder are avaliable up to $Re \approx 10^7$ [22, 23], for which drag is small, corresponding to drag crisis. In wind tunnels there is an upper limit on the size of the cylinder, and increasing the velocity eventually will make the incompressible flow model invalid, due to effects of compressibility and cavitation. To find much higher Reynolds numbers we have to consider flow problems with very large dimensions, such as geophysical flows. In the recent book [23], the case of $Re \to \infty$ is referred to as the *ultimate regime* or the *T2 regime*, which is descibed as the least known and understood state of flow, with the main reason being the lack of experimental data.

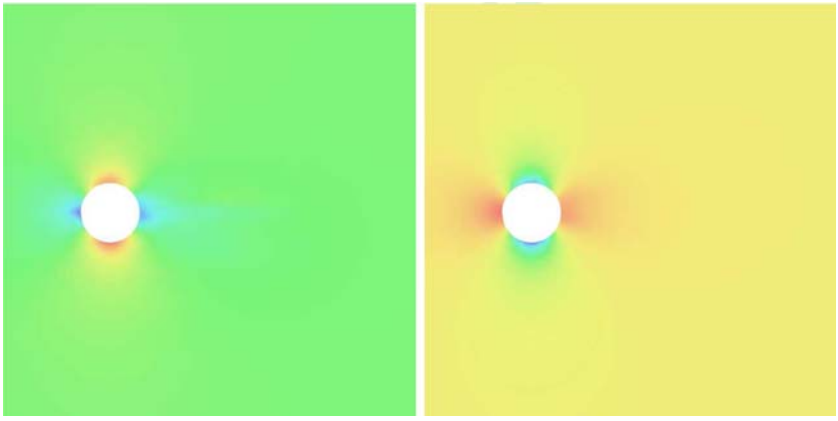

**Fig. 3** Magnitude of the velocity (*left*) and the pressure (*right*) for an EG2 solution at time $t = 0.5$, with $c_D \approx 0.1$, in the $x_1x_2$-plane for $x_3 = 0.2$

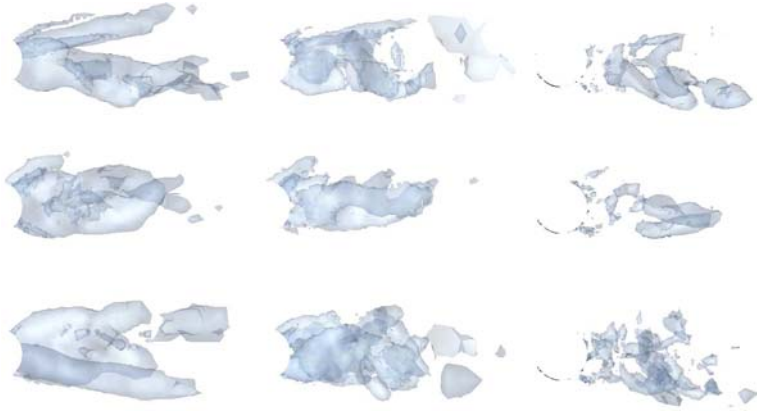

**Fig. 4** EG2: Isosurfaces for vorticity: $x_1$-component (*left*), $x_2$-component (*middle*), and $x_3$-component (*right*), at three different times (*upper, middle, lower*), in the $x_1x_2$-plane

We now consider the case of $\beta = 0$ for the cylinder. As we refine the mesh with respect to the error in drag, we find that the Euler/G2 solution (or EG2 solution) approaches the potential solution, with separation in one point (line) only, and with zero drag, see Fig. 3. But as the mesh is further refined we find that the potential solution is unstable, with the separation point generating vorticity and starting to oscillate. The oscillations are not simultaneous along the cylinder, instead there is a significant variation in the spanwise direction. The oscillating separation line generates streaks of vorticity in the streamwise direction that undergo transition to turbulence downstream the cylinder, which is shown in Figs. 4, 5 and 6, where an EG2 solution is plotted for a mesh with 75, 000 mesh points. We note that as soon as the potential solution looses stability, the drag increases and is sometimes even higher than for the case of laminar separation at $\theta \approx 90°$, see Fig. 7, where the time series of the drag for a EG2 solution on a mesh with 150, 000 nodes is shown.

The separation points generate vorticity, and sometimes structures similar to a regular von Karman vortex street, with the fundamental difference that for the EG2 solution there is separation in one point only. Indeed, studying geophysical bluff body problems, such as the flow of air past the Guadalupe Island or the Canary Islands in Fig. 9, we find that these flows appear to share the feature of separation in one point only, which is consistent with the EG2 solution, see Fig. 8, rather than in two points with a wake in between, which is the case of a standard von Karman vortex street at low Reynolds numbers [18]. A circular cylinder is of course not a realistic model of the geophysical flows in Fig. 9, which are no perfect cylinders but rather irregular 3d shapes closer to a half sphere or a surface mounted cube. Although, we believe that the computations indicate that for shapes of large dimensions, the separation may be well predicted using an EG2 model.

We note that this model is cheap since we do not have to resolve any boundary layers. The only parameter in the EG2 model is the discretization parameter $h$, and after some mesh refinement we expect the EG2 solution to be independent of $h$ with respect to certain mean value output, such as drag for example. In particular, this means that we would be able to determine the dimensionless number $c_D$ (up to a tolerance) using a computational model without any empirical constants.

The importance of a reliable model for computing incompressible flow as $Re \to \infty$ will increase as this regime is

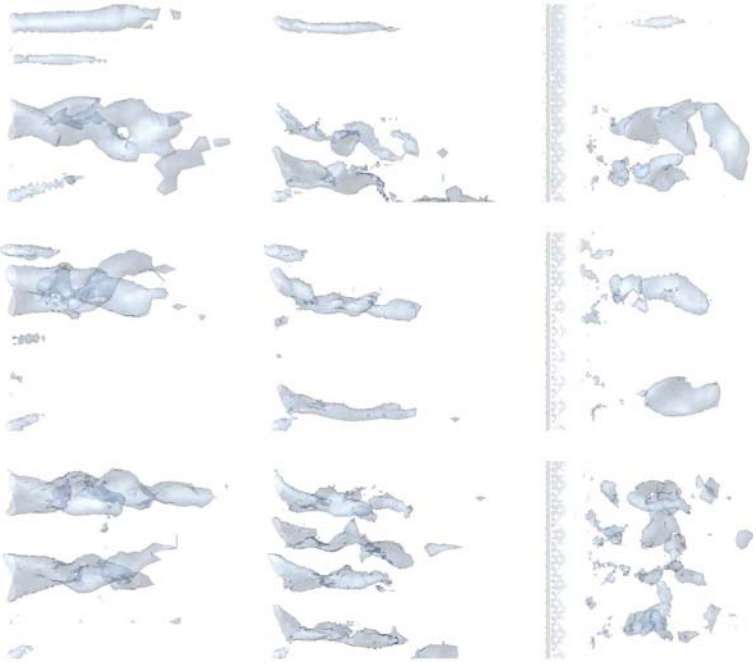

**Fig. 5** EG2: Isosurfaces for vorticity: $x_1$-component ($left$), $x_2$-component ($middle$), and $x_3$-component (right), at three different times ($upper$, $middle$, $lower$), in the $x_1x_3$-plane

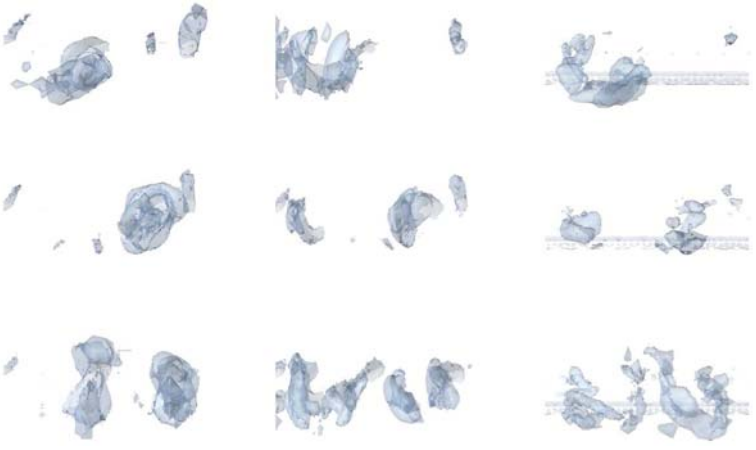

**Fig. 6** EG2: Isosurfaces for vorticity: $x_1$-component (*left*), $x_2$-component (*middle*), and $x_3$-component (*right*), at three different times ($upper$, $middle$, $lower$), in the $x_2x_3$-plane

nowadays frequently reached in civil-, offshore and wind engineering as the size of the structures increase.

## 11 Summary

We have considered the problem of computing turbulent flow past a bluff body, including the case when the boundary layers are turbulent. We have extended the G2 method to this class of problems by using a very simple wall-model in the form of a friction boundary condition, with associated friction parameter $\beta$. The idea in this paper is that for computing accurate separation, resolving the boundary layer is not crucial as long as we are able to approximate the momentum near the boundary, coupling to the skin friction of the unresolved boundary layer, which we model by the friction boundary condition.

In [4–7, 9] we find that in the case of laminar boundary layer separation we are able to capture the correct separation point (line) using G2 together with a no slip boundary condition, corresponding to $\beta \to \infty$.

Although, as the Reynolds number increases, the skin friction decreases, and the no slip boundary condition is no longer able to predict the correct flow separation. Using a no slip boundary condition, it is impossible to capture the delayed separation due to a turbulent boundary layer without a

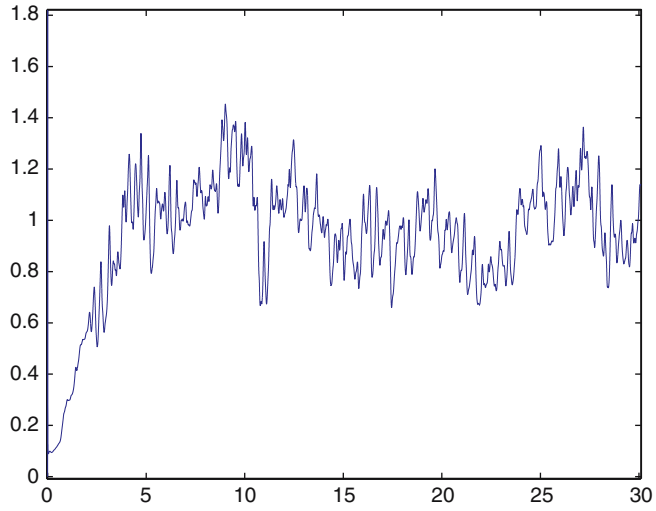


**Fig. 7** Time series of $c_D$ for an EG2 solution on a mesh with 150, 000 nodes

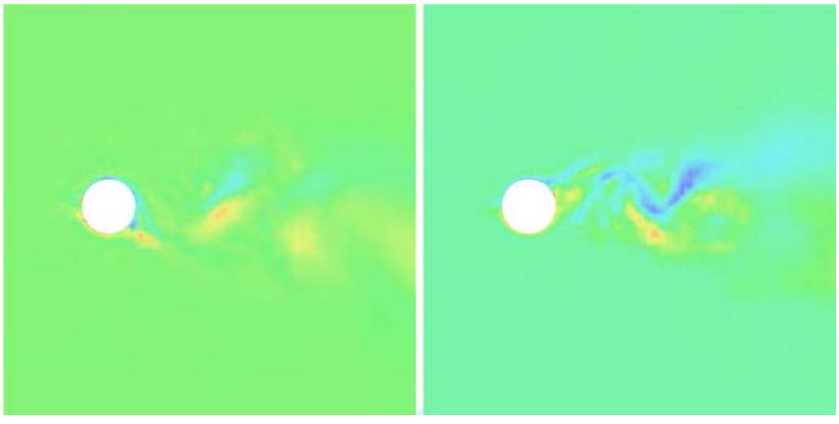

**Fig. 8** EG2: $x_3$-vorticity at two different times, in two different sections parallel to the $x_1x_2$-plane

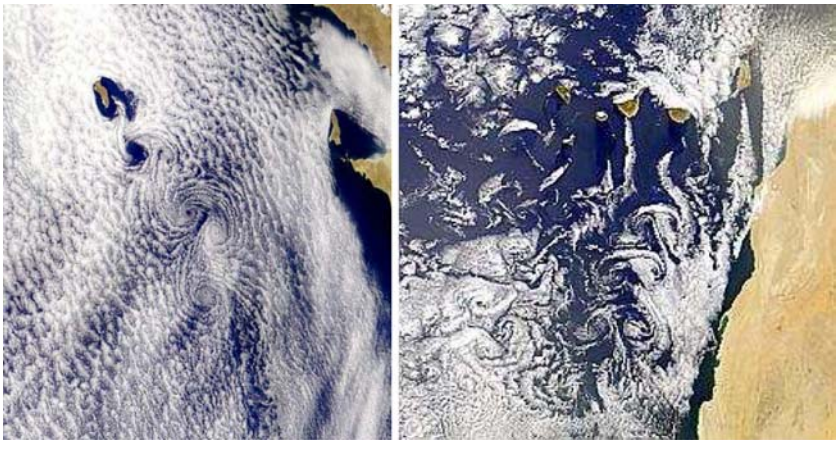

**Fig. 9** Clouds over the Guadalupe Islands (*left*) and the Canary Islands (*right*)

very high resolution of the boundary layer, which is extremely expensive. Using the friction boundary condition we can model the decreasing skin friction in a turbulent boundary layer simply by choosing a lower $\beta$.

In this paper we use G2 with a friction boundary condition to model drag crisis for a circular cylinder, where we are able to capture the delayed separation on a coarse mesh, by adjusting $\beta$ to match experimental results. From an engineering point of view it is important to take both the sub-critical and the super-critical scenario into account, and thus computations using different $\beta$ may be necessary.

We also consider the case of $Re \to \infty$ and $\beta \to 0$, corresponding to G2 for the Euler equations with slip boundary conditions, which we refer to as an EG2 method. We find that as $\beta \to 0$ for the circular cylinder the separation points (lines) move downstream until they collapse into only one single separation point (line), resembling the potential solution with zero drag. The potential solution is not stable and the single separation point (line) generates vorticity and turbulence downstream, and starts to oscillate.

That is, we have the following scenario as $\beta \to 0$ (corresponding to $Re \to \infty$) for the cylinder: (a) the laminar separation is stable for a range of Reynolds numbers ($Re \approx 10^3 - 10^5$) with drag $c_{\mathrm{D}} \approx 1.0$, (b) we then for a range of Reynolds numbers have drag crisis with a reduced wake and $c_{\mathrm{D}} \approx 0.4$ when the separation points have moved downstream, and then (c) the separation points collapse into one separation point which starts to oscillate, and generate vorticity and turbulence downstream, corresponding to high drag.

The EG2 solution corresponds to a physical flow with a very high Reynolds number, and we find flows with similar characteristics of separation in one point generating vorticity and turbulence, studying geophysical bluff body problems, such as the flow of air past the Guadalupe Island or the Canary Islands.

We note that the need of a reliable computational model for the case $Re \to \infty$ will increase, due to the large dimensions of civil-, offshore and wind engineering structures of today. EG2 is very cheap since we have no boundary layer, and we note that the EG2 model is free of any empirical parameters. For EG2 we also introduce an alternative formulation of the dual problem based on forcing data to the dual continuity equation, with the motivation of avoiding the issue of not resolving the boundary layer in the dual problem.

In future work we will extend the study of the EG2 model, and the formulation of the corresponding dual problem. We will also further investigate the friction boundary condition as a model for a turbulent boundary layer.

## References


1. Breuer M (1998) Large eddy simulation of the subcritical flow past a circular cylinder: numerical and modeling aspects. Int J Numer Methods Fluids 28: 1281–1302
2. Constantinescu G, Squires K (2004) Numerical investigations of flow over a sphere in the subcritical and supercritical regimes. Phys Fluids 16(5):1449–1466
3. Frisch U (1995) Turbulence — the legacy of A. N. Kolmogorov. Cambridge University Press, Cambridge
4. Hoffman J (2005) Adaptive simulation of the turbulent flow due to a cylinder rolling along ground. Comput Methods Appl Mech Engng (under review)
5. Hoffman J (2005) Computation of mean drag for bluff body problems using adaptive dns/les. SIAM J Sci Comput 27(1):184–207
6. Hoffman J (2005) Efficient computation of mean drag for the subcritical flow past a circular cylinder using general galerkin g2. Int J Numer Methods Fluids (in press)
7. Hoffman J (2006) Adaptive simulation of the turbulent flow past a sphere. J Fluid Mech (in press)
8. Hoffman J, Johnson C (2006) Computational turbulent incompressible flow: applied mathematics body and soul, Vol 4. Springer, Berlin Heidelberg, New York
9. Hoffman J, Johnson C (2006) A new approach to computational turbulence modeling. Comput Methods Appl Mech Engrg (in press)
10. Iliescu T, John V, Layton WJ (2002) Convergence of finite element approximations of large eddy motion. Numer Method Part Diff Equ 18:689–710
11. John V (2002) Slip with friction and penetration with resistance boundary conditions for the navier–stokes equations — numerical tests and aspects of the implementation. J Comp Appl Math 147:287–300
12. John V, Layton WJ, Sahin N (2003) Derivation and analysis of near wall models for channel and recirculating flows. Comput Math Appl (in press)
13. John V, Liakos A (2005) Time dependent flow across a step: the slip with friction boundary condition. Int J Numer Methods Fluids (in press)
14. Krajnović S, Davidson L (2002) Large-eddy simulation of the flow around a bluff body. AIAA 40:927–936
15. Kravchenko AG, Moin P (2000) Numerical studies of flow over a circular cylinder at $re_d = 3900$. Phys Fluids 12(2):403–417
16. Maxwell JC (1879) Phil. Trans. Royal Society
17. Mittal R (1996) Progress on les of flow past a circular cylinder. Center for Turbulence Research Annual Research Briefs
18. NASA (2005) Various views of von karman vortices. http://www.disc.gsfc.nasa.gov/oceancolor/scifocus/oceanColor/von-Karman_vortices .shtml
19. Navier CLMH (1823) Mémoire sur les lois du mouvement des fluiales. Mém Acad R Soc 6:389–440
20. Rodi W, Ferziger JH, Breuer M, Pourquié M (1997) Status of large eddy simulation: results of a workshop. ASME J Fluids Eng 119:248–262
21. Sagaut P (2001) Large Eddy simulation for incompressible flows. Springer, Berlin Heidelberg New York
22. Schlichting H (1955) Boundary layer theory. McGraw-Hill, New York
23. Zdravkovich MM (1997) Flow around circular cylinders: a comprehensive guide through flow phenomena, experiments, applications, mathematical models, and simulations, vol 1 [Fundamentals]. Oxford University Press, Oxford